ACTUATOR INFLUENCE ON FLYING QUALITIES OF A NATURALLY UNSTABLE AIRCRAFT

Alexander P. Feuersänger, Carsten Döll, Clément Toussaint
ONERA-CERT/DCSD
Systems Control and Flight Dynamics Department
BP 4025, F-31055 Toulouse Cedex, France

Keywords: *Reduced stability, actuator activity, saturation, fatigue*

Abstract

This paper addresses the interplay of actuator properties and reduced longitudinal stability of a civil aircraft. The considered aircraft is the future concept VELA (Very Efficient Large Aircraft) which is very sensitive to centre of gravity displacements. A simple feedback controller scheduled as a function of the centre of gravity position guarantees modal handling quality specifications for a wide range of positions. Special interest is laid on aft positions because these reduce the longitudinal stability and impose a demanding task on the elevator actuator. Limits of c.o.g. positions are inferred from the interrelation of handling qualities, fluctuation of actuator deflection and slew rate during flight in turbulent atmosphere and fatigue inflicted upon the actuator.

1 Introduction

Civil aircraft have undergone a significant change in terms of their flight mechanic conception. To ensure controllability, civil aircraft were designed to be naturally stable in the whole flight domain. With the technological advance though, today's developments seek to reduce natural stability because this allows for the use of smaller stabilising surfaces, reducing mass and drag, and thus also the impact on the environment. As a consequence, the natural aircraft with reduced stability does not necessarily meet the handling quality requirements for certification. Therefore, a control system has to be installed which guarantees the minimal specifications for certification.

Rather than focusing on the definition of the stabilising control system, this paper examines the interplay of control surface actuators and an artificially stabilised aircraft. The considered aircraft is the future concept VELA1, which was developed within the framework of a European research project. It represents a two-tailed blended wing-body configuration that surpasses the current A380 in mass/capacity as well as in geometry specifications.

The VELA1 concept is very sensitive to centre of gravity (c.o.g.) displacements [1]. This affects trimming the aircraft as well as controlling it. The latter poses a demanding task for the elevator actuator when considering aft c.o.g. positions (X_g) [2].

The closed-loop behaviour of the aircraft short-period oscillation (SPO) is scrutinised for flight in turbulent atmosphere during take-off and approach, i.e. low speed, as these flight phases are critical w.r.t. handling qualities. The expected command fluctuations due to the controller are examined and fatigue and damage caused therewith are determined.

The paper is organised as follows. Section II presents modelling aspects, section III gives the theoretical background and poses the problem with the application to the aircraft. Theory is given on the calculation of fluctuations evoked by random signals in linear systems as well as on

fatigue and damage inflicted on actuators under strain. Section IV presents the results and concluding remarks end the paper.

2 Aircraft and atmosphere modelling

In this section, the aerodynamic and flight mechanics models are introduced. For the aerodynamic model, validated numerical data which ensure modelling at a very detailed level were directly drawn from the VELA project. For the flight mechanics model, the general rigid body equations of motion are considered [10]. The aircraft has a mass range $M \in [550\,t, 770\,t]$ with a nominal inertia $I_{yy,nom} = 44.8 \cdot 10^6\,kgm^2$. Reference data is listed in Table 1.

Reference surface	S	=	2012	m^2
Mean aerodynamic chord (≡ Reference length)	l	=	35.93	m
Wing span	b	=	99.60	m

Table 1 VELA reference values

2.1 Equations

The rigid body flight mechanics equations are expressed in the body frame coordinate system. The angular velocities of the aircraft are defined by the vector $\vec{\Omega} = (p,q,r)^T$, with p being the roll rate, q the pitch rate and r the yaw rate.

With $\vec{V}$ being the velocity vector of the aircraft in aircraft coordinates and $\vec{h} = J\vec{\Omega}$ the angular momentum (where J is the tensor of inertia), the dynamic equations are:

$$m\dot{\vec{V}} = \Sigma\vec{F}_{ext} + m\vec{\Omega}\times\vec{V} + m\vec{g} \quad (1)$$

$$J\dot{\vec{\Omega}} = \Sigma\vec{M}_{ext} + \vec{\Omega}\times(J\vec{\Omega}) \quad (2)$$

The external forces $\vec{F}_{ext}$ and moments $\vec{M}_{ext}$ exerted on the aircraft come from aerodynamic loads $(\vec{F}_{aero}, \vec{M}_{aero})$ and thrust loads $(\vec{F}_{thr}, \vec{M}_{thr})$. With the dimensionless aerodynamic coefficients, the aerodynamic loads read:

$$F_{aero} = \frac{1}{2}\rho S V_{aero}^2 \begin{pmatrix} C_X \\ C_Y \\ C_Z \end{pmatrix} \quad (3)$$

$$M_{aero} = \frac{1}{2}\rho S l V_{aero}^2 \begin{pmatrix} C_L \\ C_M \\ C_N \end{pmatrix} \quad (4)$$

where S and l are the reference area and reference length, ρ the density of the ambient air and V_{aero} the aerodynamic speed. The coefficients are described in the body frame. The inertia tensor is symmetric with respect to the aircraft symmetry plane (x,z) and reads:

$$J = \begin{pmatrix} A & 0 & -E \\ 0 & B & 0 \\ -E & 0 & C \end{pmatrix} \quad (5)$$

For the complete description of the model, the equations for pitch angle θ, yaw angle ϕ, heading ψ and the kinematic equation for the vertical speed were also implemented. After a change of variables, one obtains the state vector with the nine state variables:

$$X = (V, \alpha, \beta, \theta, \phi, p, q, r, h)^T \quad (6)$$

The outputs of the model include the load factors n_X, n_Y and n_Z in the body frame.

2.2 The aerodynamic model

The aerodynamic data are tabulated and allow for the reconstruction of all six aerodynamic coefficients (C_X, C_Y, C_Z, C_L, C_M and C_N). These are functions of the angle of attack α successively combined with yaw angle β, rotational velocities p, q and r, accelerations $\dot{\alpha}$ and $\dot{\beta}$, and finally the control surface deflections (elevator, rudders - left and right - and wing control surfaces A1 to A10 - ailerons and spoilers)[1].

The aerodynamic data are given for the reference point X_{ref} which is placed at 30.7% of the mean aerodynamic chord l. The model is parametrised as a function of the dimensionless c.o.g. displacement dx_g along the x-axis:

$$dx_g = \frac{X_g - X_{ref}}{l} \quad (7)$$

[1] Only the elevator is used in this paper.

2.3 Equilibrium and linearisation

The equilibrium is chosen to be straight, level, symmetric flight at zero altitude h (take-off, approach), low speed (Mach = 0.2), mass $M = 550t$ and with $\dot{h} = V_z = 0\,m/s$. The system dynamics can be linearised about the equilibrium ($f(X_{eq}, u_{eq}) = 0$) as follows:

$$\begin{aligned} \dot{X} = \quad f(X,u) \quad &\approx f(X_{eq},u_{eq}) + \\ &\left.\frac{\partial f}{\partial X}\right|_{X_{eq},u_{eq}} \bar{X} + \left.\frac{\partial f}{\partial u}\right|_{X_{eq},u_{eq}} \bar{u} \\ Y = \quad g(X,u) \quad &\approx g(X_{eq},u_{eq}) + \\ &\left.\frac{\partial g}{\partial X}\right|_{X_{eq},u_{eq}} \bar{X} + \left.\frac{\partial g}{\partial u}\right|_{X_{eq},u_{eq}} \bar{u} \end{aligned} \tag{8}$$

with $\bar{X} = X - X_{eq}$ ($\dot{\bar{X}} = \dot{X}$) and $\bar{u} = u - u_{eq}$. This leads to:

$$\begin{aligned} \dot{\bar{X}} &= A\bar{X} + B\bar{u} \\ \bar{Y} &= C\bar{X} + D\bar{u} \end{aligned} \tag{9}$$

with $\bar{Y} = Y - Y_{eq}$.
The partial derivatives $\frac{\partial f}{\partial X}, \ldots$ are calculated using the centered difference quotient:

$$\frac{\partial f}{\partial X_i}(X,u) = \frac{f(X + \varepsilon e_i, u) - f(X - \varepsilon e_i, u)}{2\varepsilon} \tag{10}$$

where e_i is the vector of the i-th component of the state vector X. ε gives the precision and is set to 10^{-4}.

For the sake of legibility the 'bars' will be omitted in future reference.

2.4 Actuator model

In this subsection, we briefly give the linear transfer used to model the elevator actuator of the aircraft:

$$H_{act}(p) = \frac{1}{T_{act}\,p + 1}. \tag{11}$$

This model has been chosen for two reasons. Firstly, the model behaviour in terms of frequency and step response is comparable to a fairly exact model provided by the industry when the actuator time constant is set to $T_{act} = 0.06\,s$. Secondly, this simple parametrisation allows for clear and interpretable results as regards actuator bandwidth[2] needs.

2.5 Model of the turbulent atmosphere

Flight in turbulent atmosphere can be modelled with the help of a random signal (Gaussian white noise) at the input of the linearised aircraft. This random signal is filtered by a transfer incorporating the atmospheric properties. A spectral Dryden representation (12) (i.e. the energies of the horizontal and vertical speeds of the turbulent atmosphere are functions of frequency) facilitates simulation and analysis:

$$\begin{aligned} \Phi_{Wx}(\omega) &= \frac{2\sigma_x^2 L_x}{\pi V} \cdot \frac{1}{1 + \left(L_x \frac{\omega}{V}\right)^2} \\ \Phi_{Wz}(\omega) &= \frac{\sigma_z^2 L_z}{\pi V} \cdot \frac{1 + 3\left(L_z \frac{\omega}{V}\right)^2}{\left[1 + \left(L_z \frac{\omega}{V}\right)^2\right]^2} \end{aligned} \tag{12}$$

ω is the frequency in rad/s, L_x and L_z are characteristic scale lengths of the turbulence in x and z direction, respectively. σ_x and σ_z (turbulence intensity) are the associated standard deviations. Normalising these spectra yields:

$$\int_0^\infty \Phi_{W_{x/z}}(\omega)\,d\omega = \sigma_{x/z}^2. \tag{13}$$

The atmospheric conditions in our case are set to stormy conditions and are characterised by the following values:

$$L_x = L_z = 50\,m \quad \text{and} \quad \sigma_x = \sigma_z = 5\,m/s. \tag{14}$$

3 Determination of actuator activity and fatigue

This section provides the theoretical background needed to determine the actuator activity and fatigue related to a given equilibrium point depending on Mach number, altitude and position of the centre of gravity.

[2] The time constant T of a first order transfer with DC gain 1 is related to its bandwidth bw via $bw \approx [0; \omega_c]$ with $\omega_c = T^{-1}$.

3.1 Passage of a random signal through a linear system

Consider a linear system whose input is a white Gaussian noise w. Then its state x and output y are also random signals. If the deterministic input is $u(t) = 0$, we can state the following theorem [9]:

Consider a linear system:

$$\dot{x}(t) = Ax(t) + Mw(t) \tag{15}$$

where $w(t)$ is a stationary white Gaussian noise with a power spectral density W. $m(t_0)$ represents the mean and $P(t_0)$ the covariance of the initial random state $x(t_o)$. Therefore, $x(t)$ is also a random signal

– with mean

$$m(t) = E[x(t)] = e^{(A(t-t_0))} m(t_0) \tag{16}$$

– and covariance

$$P(t) = E[(x(t) - m(t))(x(t) - m(t))^T]. \tag{17}$$

These fulfill the differential equation:

$$\dot{P}(t) = AP(t) + P(t)A^T + MWM^T. \tag{18}$$

Assuming that the system is asymptotically stable it will tend towards steady-state behaviour. Therefore $\dot{P} = 0$ and $P(t) = P$. This yields the Lyapunov equation:

$$AP + PA^T + MWM^T = 0 \tag{19}$$

The output equation of the linear system $y(t) = Cx(t)$ delivers the covariance matrix $S(t)$ of output $y(t)$:

$$S(t) = CP(t)C^T \tag{20}$$

In steady state, with $\dot{S} = 0$ and $S(t) = S$, the standard deviation of the i-th state variable is the square root of the i-th diagonal element of S:

$$\sigma_i^2 = S_{ii} \tag{21}$$

3.2 Theory of fatigue and damage

3.2.1 Sinusoidal stress

Consider a material exposed to stress $e(t)$ (for example compression or torsion). The damage to a sinusoidal prompting

$$e(t) = \sigma \sin(\omega t + \phi)$$

of amplitude (level) σ which is repeated during n cycles is

$$d = \frac{n}{N} \tag{22}$$

where N is the maximum number of cycles at level σ causing the first crack or finally the rupture. N is usually given by the well–known Wöhler curves, see for example [4].

We are interested in the so called *area of fatigue* of the Wöhler curve. The stress on the component does not cause plastic deformations but the repeated application debases the structure of the material and triggers earlier or later the appearance of the first crack. The Basquin law,

$$N\sigma^b = C, \tag{23}$$

is an analytical approximation for the Wöhler curve within the fatigue area. It depends on two material constants b and C[3].

One of the most commonly used rules to estimate the overall damage is the Palmgren–Miner theorem [4]. It states that the overall damage D is the sum of the damages d_i at different levels

$$D = \sum_i d_i = \sum_i \frac{n_i}{N_i} \tag{24}$$

which means that rupture occurs when $D = 1$.

3.2.2 Stochastic stress

Following [8], the Palmgren–Miner theorem (24) becomes the mean damage D

$$D = T\, n_p^+ \int_0^{+\infty} \frac{q(\sigma)}{N(\sigma)}\, d\sigma \tag{25}$$

[3]The material is assumed to be aluminium 6144 T4 with dimensionless constants $b = 14.0$ and $C = 2.26 \cdot 10^{78}$.

for a stochastic stress $e(t)$ applied during the time span T and with a probability density $q(\sigma)$ for the occurrence of a positive extremum of level σ. The mean number of positive extrema during T is called $T\,n_p^+ = T\int_0^{+\infty} q(\sigma)\,d\sigma$. Using the Basquin law, (25) becomes

$$D = \frac{T\,n_p^+}{C}\int_0^{+\infty} \sigma^b\,q(\sigma)\,d\sigma \qquad (26)$$

It can be shown [5], that the density function $q(\sigma)$ for a Gaussian $e(t)$ is a combination of a Gaussian law $G(0,\sqrt{1-r^2})$ and a Rayleigh law $R(1)$ with the irregularity factor r as parameter.

Assuming that the signal is very regular, i.e. $r \approx 1$ and hence $q(\sigma)$ a Rayleigh law, (26) retrieves to

$$D \approx \frac{T\,n_p^+}{C}\left(\sqrt{2}\sigma_e\right)^b \Gamma\left(1+\frac{b}{2}\right) \qquad (27)$$

with σ_e the standard deviation of $e(t)$. In fact, this approximation is even still valid for small r. It will be used further on.

Assuming that the signal is irregular, i.e. $r = 0$, $q(\sigma)$ is Gaussian, n_p^+ can be easily evaluated via

$$n_p^+ = \frac{1}{2\pi}\frac{\sigma_{\dot{e}}}{\sigma_e} \qquad (28)$$

Combining (28) and (27) delivers finally the relation of the mean damage D during T

$$D \approx \frac{T}{2\pi C}\sqrt{2}^b\,\Gamma\left(1+\frac{b}{2}\right)\sigma_{\dot{e}}\,\sigma_e^{b-1} \qquad (29)$$

i.e. the mean damage D due to $e(t)$ depends on the standard deviation of $e(t)$ and the standard deviation of $\dot{e}(t)$.

3.2.3 *Impact on the actuator*

The considered failure case of the elevator actuator is the rupture of the hydraulic jack due to stress. The stress e is hence the force acting on the jack F_j divided by its section S_j

$$e = \frac{F_j}{S_j}.$$

The force F_j on the jack is given by the lever arm c_j between the jack and the elevator surface and the aerodynamic hinge moment M_{hinge} applied at the control surface:

$$e = \frac{M_{hinge}}{S_j\,c_j}$$

Like M_{aero} in (3), the hinge moment M_{hinge} is also a function of the aerodynamic pressure ρV^2, the reference surface S, the mean aerodynamic chord l and the deflection of the control surface δm. It also depends on the Mach number Ma and the configuration of the aircraft, $conf$. In a first linear approximation for M_{hinge}, it can be written

$$e \approx \frac{\frac{1}{2}\rho V^2 S\,l\,f(Ma,conf)\,\delta m}{S_j\,c_j} \approx K\,\delta m \qquad (30)$$

which means that the stress e is almost proportional w.r.t. δm. Because of this linearity, the standard deviations of e, $\dot{e}$ are also proportional w.r.t. the standard deviations of δm and $\dot{\delta m}$. The mean damage (29) can hence approximately be expressed by the deflection δm and its speed $\dot{\delta m}$ as follows:

$$D \approx K_g\,\sigma_{\dot{\delta m}}\,\sigma_{\delta m}^{b-1} \qquad (31)$$

with

$$K_g = \frac{T}{2\pi C}\Gamma\left(1+\frac{b}{2}\right)\left(\sqrt{2}K\right)^b \qquad (32)$$

and

$$K = \frac{S}{S_j}\frac{l}{c_j}\frac{1}{2}\rho V^2\,f(Ma,conf) \qquad (33)$$

as shown in [8, 6].

The standard deviations of δm and $\dot{\delta m}$ have already been determined with (19) and (20) by a Lyapunov analysis of the closed-loop aircraft system. Hence, the associated damage can be directly computed using (31)–(33).

3.2.4 *Accumulated damage*

As shown in [8, 6], a flight mission can be divided in several phases i, each characterised by a certain aircraft model, control law, flight conditions and stochastic filters W_i modelling the main excitations. Again, white Gaussian noise is the input. As the damage is cumulative (as shown before), it suffices to evaluate each mean damage D_i

separately using (29) and to sum the D_i to obtain the mission damage $D_{mission}$ using some weighting factors w_i. The latter represent the time spent within the flight phase i compared to the total mission duration.

The weighting factors with regard to turbulence can also be determined, when considering probabilistic data, as in [3]. Turbulence of a certain deviation σ_{turb} are assumed to appear with a certain probability P_σ. This value multiplied with the total service time of an aircraft T_{total} gives the time during which the aircraft is probably exposed to a certain type of turbulence. Thus, one obtains a weighting factor of the examined damage-type compared to the aircraft service life.

Nevertheless, the analysis will be limited in this paper to the take-off and approach phases, whose conditions where described in sections 2.3 and 2.5. The accumulated damage will not be shown, but a relative damage D_N is presented which depends on the c.o.g. position, and hence on the degree of natural stability. It represents the damage at X_g normalised by the damage at the reference point X_{ref}: $D_N = \frac{D_{Xg}}{D_{Xref}}$.

3.3 Application to the aircraft

3.3.1 Variables influenced by turbulence

The aerodynamic speed V_{aero} is composed of the inertial speeds v_x and v_z in combination with the wind components W_x and W_z:

$$\begin{aligned} v_{aX} &= v_X - W_x\cos\theta + W_z\sin\theta \\ v_{aZ} &= v_Z - W_x\sin\theta - W_z\cos\theta \end{aligned} \quad (34)$$

and hence

$$V_{aero} = \sqrt{v_{aX}^2 + v_{aZ}^2} \quad (35)$$

$$\alpha_{aero} = \tan^{-1}\left(\frac{v_{aZ}}{v_{aX}}\right) \quad (36)$$

For small wind perturbations, the linearised expression for variables speed V_{aero} and angle of attack α_{aero} read:

$$V_{aero} = V - W_x\cos\gamma + W_z\sin\gamma \quad (37)$$

$$\alpha_{aero} = \alpha - \frac{W_z}{V}\cos\gamma - \frac{W_x}{V}\sin\gamma \quad (38)$$

In order to render the model more precise, the gradient of the vertical wind is taken into account, which has an effect onto the pitch rate of the aircraft. The pitch rate then becomes:

$$\begin{aligned} q_a &= q + q_w \quad \text{where} \\ q_w &= -(\dot\alpha - \dot\alpha_{aero}) \\ &= -\frac{\dot W_z}{V}\cos\gamma - \frac{\dot W_x}{V}\sin\gamma \end{aligned} \quad (39)$$

The wind component in z-direction produced by this extra wind pitch rate is added to W_z by the means of a transfer (pseudo-derivation)

$$H_{qw}(p) = \frac{p}{1+\tau_{qw}p} \quad \text{with} \quad \tau_{qw} = \frac{4b}{\pi V}, \quad (40)$$

where the size of the aircraft is taken into account via its wing span b.

3.3.2 The complete linearised model

The focus of this paper is on the SPO, which can be extracted from the full state-space representation of section 2.3. A reduced three-state longitudinal system (aircraft states α and q and actuator state δm) with vertical wind (w) and elevator (δm) as inputs is obtained:

$$\begin{aligned} \dot x_{red} &= A_{red}\,x_{red} + B_{red}\,u \\ y_{red} &= C_{red}y_{red} + D_{red}\,u \end{aligned} \quad (41)$$

with

$$x_{red} = \begin{pmatrix} \alpha \\ q \\ \delta m \end{pmatrix} \quad y_{red} = \begin{pmatrix} \alpha \\ q \end{pmatrix} \quad u = \begin{pmatrix} w \\ \delta m \end{pmatrix}$$

As the model has especially been parametrised as a function of X_g, this reduced system can be systematically calculated for each c.o.g. displacement dx_g within the considered target range. Static feedback controllers $\delta m = (K_\alpha, Kq)\cdot(\alpha, q)^T$ have been synthesized for each X_g assuring the specifications for the SPO in Table 2.
These values were chosen in order to be compliant with the military specifications MIL-STD-1797 [7], assuring minimum handling

Damping ratio ξ	Frequency ω
0.3 / 0.7	0.8 rad/s

Table 2 SPO specifications.

qualities during take-off and landing (damping ratio $\xi = 0.3$). A second, higher damping ($\xi = 0.7$) is also considered as to identify the influence of the modal specifications for the basic control law.

The loop between aircraft states $[\alpha, q]$ and elevator input δm can now be closed and the complete linearised system can be rewritten as:

$$\underbrace{\begin{pmatrix} \dot{X}_w \\ \dot{X}_{CL} \end{pmatrix}}_{\dot{X}_{CLw}} = \underbrace{\begin{pmatrix} A_w & 0 \\ B_{CL}C_w & A_{CL} \end{pmatrix}}_{A_{CLw}} \underbrace{\begin{pmatrix} X_w \\ X_{CL} \end{pmatrix}}_{X_{CLw}} + \underbrace{\begin{pmatrix} B_w \\ 0 \end{pmatrix}}_{B_{CLw}} e_w$$
$$\underbrace{\begin{pmatrix} u_w \\ Y_{CL} \end{pmatrix}}_{Y_{CLw}} = \underbrace{\begin{pmatrix} C_w & 0 \\ D_{CL}C_w & C_{CL} \end{pmatrix}}_{C_{CLw}} \underbrace{\begin{pmatrix} X_w \\ X_{CL} \end{pmatrix}}_{X_{CLw}} \quad (42)$$

The subscripts CL and w denote the matrices and vectors associated to the closed-loop system and to the wind, respectively, where the only system input is the Gaussian white noise e_w.

3.3.3 *Actuator activity and fatigue*

The newly obtained system matrices A_{CLw}, B_{CLw} and C_{CLw} are now considered for the calculation of the standard deviations. The Lyapunov equation (19) then becomes:

$$A_{CLw}P + PA_{CLw}^T + B_{CLw}B_{CLw}^T = 0 \quad (43)$$

The covariance matrix is derived from (44), which is evaluated for all dx_g in the range of interest $[-10\,\%; 10\,\%]$.

$$S = C_{CLw}PC_{CLw}^T. \quad (44)$$

With the help of these deviations calculated for specific flight conditions, we can infer the actuator activity as a function of dx_g as well as of the actuator time constant T_{act}.

4 Results

This section is dedicated to the presentation of the results. In a first step, the evolution of the necessary gains on the aircraft states $[\alpha, q]$ is detailed. In a second step, the related actuator activity (in position and rate) is presented, from where we will derive the damage increment inflicted upon the actuator.

4.1 Gain vs X_g

The necessary gain to guarantee the SPO specifications depends on the specifications themselves as well as on the c.o.g. position X_g of the linearised aircraft and the selected actuator time constant T_{act}. Fig. 1 shows this relation for a fixed damping ratio $\xi = 0.3$.

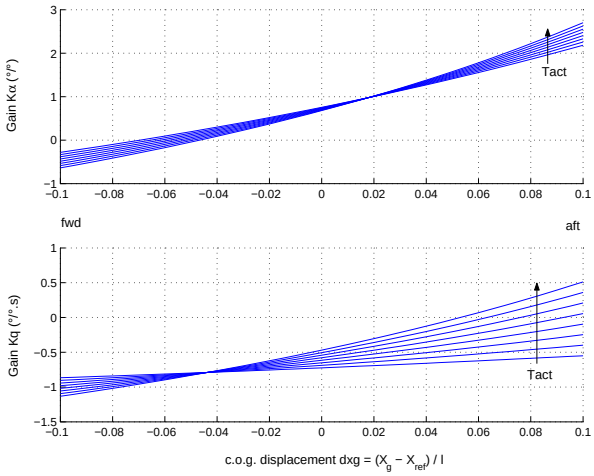

Fig. 1 Gains K_α, K_q as a function of X_g and T_{act}, $\xi = 0.3$.

As expected, the gain K_α rises with aft X_g as it predominantly affects the SPO frequency/module. The linearised poles of the natural aircraft tend to become aperiodic with aft X_g and to lose on the degree of stability λ[4] and hence on the module which needs to be compensated by the gain. The actuator bandwidth causes small changes in gain. As concerns the gain in K_q, which plays a major role w.r.t. the SPO damping, the impact of the actuator bandwidth is stronger: it can even cause a change of the algebraic sign of the necessary gain in order to obtain the same pole placement.

[4]The degree of stability of a state matrix A is $-\max_i \mathrm{Re}(\lambda_i)$, where the λ_i are the eigenvalues of A.

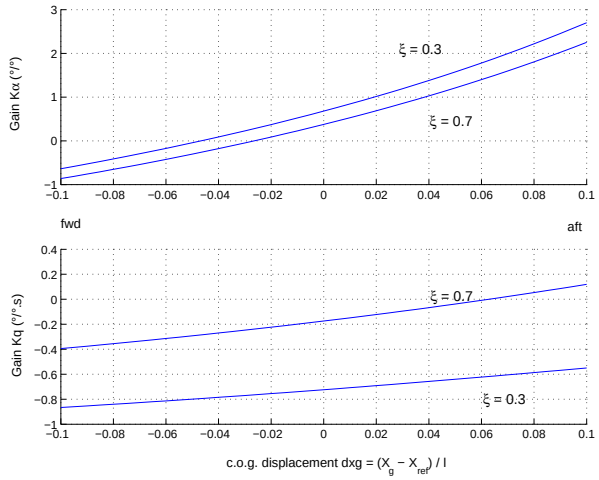

Fig. 2 Influence of modal specifications on gains. $T_{act} = 0.06\,s$, $\xi = 0.3/0.7$.

Remark: Based on the assumption that K_α tunes the system frequency ω and K_q modifies the system damping ξ, it is interesting to state the following: Fig. 1 shows us that there exist X_g for which the actuator does not have an influence on the frequency of the system and others for which there is no actuator influence on the system damping.

With T_{act} fixed, the effect of the choice of the imposed damping is visualized in Fig. 2. The choice of a higher damping does, contrarily to the expected, reduce the norm of the gains. This fact becomes clearer when recalling the natural behaviour of the SPO poles. From being periodic for forward dx_g with damping ratio $\xi \approx 0.3$, the poles become aperiodic ($\xi = 1$) for $dx_g \approx 0$, i.e. $X_g \approx X_{ref}$, and unstable for $dx_g > +2\%$. This states that the natural damping ratio is quite high throughout a large part of the X_g-range, and hence less energy (gain) is needed to impose a damping ratio of 0.7 than for 0.3 with the same fixed frequency of $0.8\,rad/s$. In other words, choosing minimal handling qualities may not be the best choice in order to obtain minimal gains.

4.2 Activity vs. X_g

As the considered aircraft (VELA) does not have a separate horizontal plane for trimming, the elevator is used to maintain the equilibrium. Thus, deviations of the elevator deflection in turbulent flight have to be added to the initial trim deflection.

Deflection or rate deviations are plotted for 1σ (dashed), covering 68 % of all fluctuations expected to be encountered, and 3σ (continuous) covering 99.7 %. These are functions of X_g and the actuator time constant. Red lines denote an actuator time constant of $T_{act} = 0.06\,s$.

Vertical dashed lines indicate two c.o.g. positions of interest: position of manoeuvre point and zero static margin point. Horizontal continuous lines indicate typical values for saturation in position and rate of the elevator actuator.

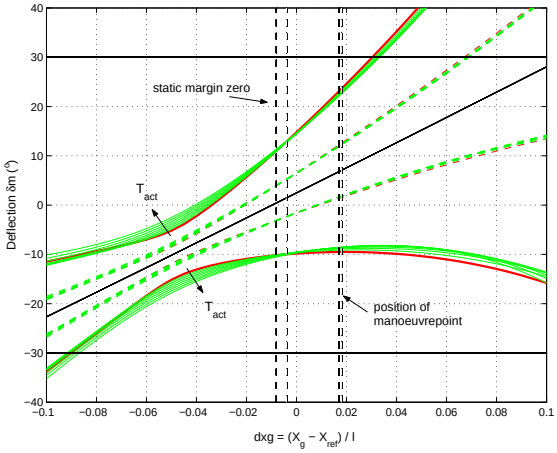

Fig. 3 Boundaries of the elevator deflection δm. $T_{act} \in [0.06\,s; 0.48\,s]$.

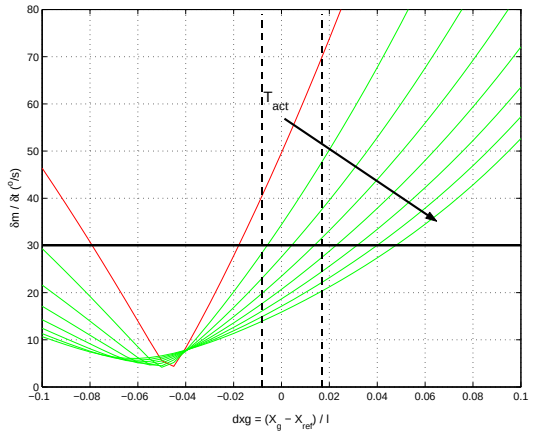

Fig. 4 Boundaries of the actuator rate $\delta\dot{m}$. $T_{act} \in [0.06\,s; 0.48\,s]$.

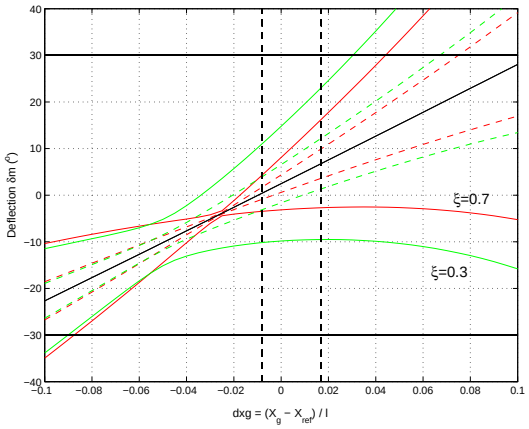

Fig. 5 Influence of modal specification onto elevator deflection boundaries. $T_{act} = 0.06\,s$. Red: $\xi = 0.7$, green: $\xi = 0.3$.

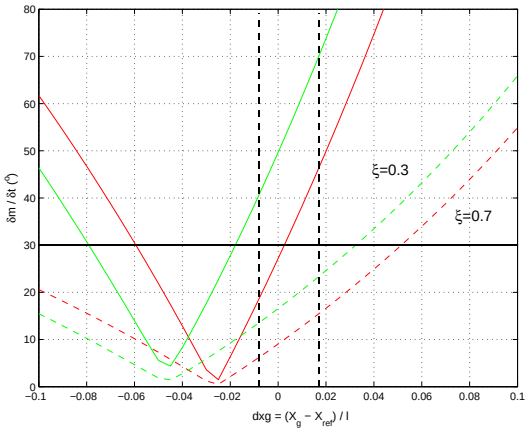

Fig. 6 Influence of modal specification onto elevator rate boundaries. $T_{act} = 0.06\,s$. Red: $\xi = 0.7$, green: $\xi = 0.3$.

Fig. 3 displays the sum of elevator trim deflection and deviations with the modal specification $\xi = 0.3$. We can infer limits for the allowable X_g displacement dx_g, with 9% forward and 3% on aft, according to where the deviations disrespect saturation constraints. The impact of the parameter T_{act} is negligible.

Fig. 4 shows the actuator rate fluctuations for $\xi = 0.3$. The effect of the parameter T_{act} is very clear. A rapid actuator causes higher rate fluctuations and hence a very small range of X_g, whereas a slower actuator can widen the allowable c.o.g. range clearly. The actuator plays the role of a filter. Still, nonlinear simulations show that values of $T_{act} > 0.2\,s$ cause a significant loss in manoeuvre handling quality. The resulting X_g-range is much tighter. A recommendation for an actuator with a higher slew rate saturation can be given.

Figs. 5 and 6 demonstrate the influence of the choice of the imposed damping ratio ξ: the X_g with minimum fluctuation is moved aft for a higher damping ratio ($\xi = 0.7$). As concerns actuator rate, a higher damping ratio shifts the range of allowable X_g to aft positions, but does not influence its size. With regard to fluctuations in position though, a higher damping can reduce fluctuation and therefore widen the accessible c.o.g. area.

4.3 Damage vs. X_g

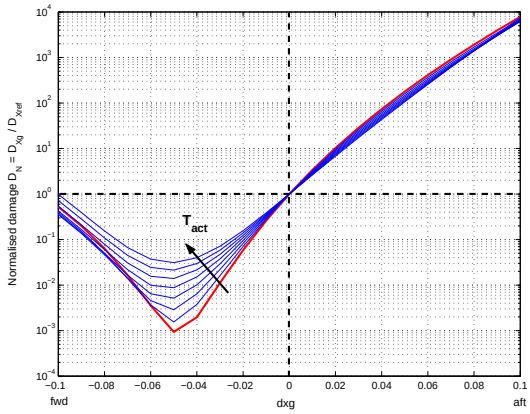

Fig. 7 Normalised damage $D_N = \frac{D_{Xg}}{D_{Xref,\xi=0.3}}$ as a function of dx_g. $\xi = 0.3$, $T_{act} \in [0.06\,s; 0.48\,s]$. Red (thick): $T_{act} = 0.06\,s$.

Fig. 7 shows the normalised damage D_N for each c.o.g. displacement dx_g. The data are displayed logarithmically and show the enormous increase in damage for extreme aft X_g. The actuator time constant influence is visible and allows for damage differences of order 10^1 to 10^2 for forward X_g. The mean damage rises with a higher T_{act}, which becomes clear when recalling that deviations in position δm cause significantly higher damage than those in rate $\delta\dot{m}$. Compare with (31) and Figs. 3, 4.

Fig. 8 demonstrates the impact of the choice of the imposed damping ratio for a fixed T_{act}. For the sake of comparability, the damage values for

damping ratio $\xi = 0.7$ have been normalised with $D_{Xref,\xi=0.3}$ as well. Damage is notably lower for all displacements dx_g more aft than -4%. Only extreme forward positions incorporate damage higher than the $\xi = 0.3$ case.

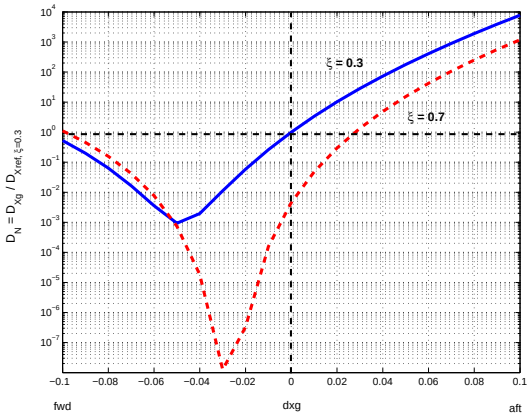

Fig. 8 Influence of modal specifications on D_N. Normalised with $D_{Xref,\xi=0.3}$. $T_{act} = 0.06s$. Blue (continuous): $\xi = 0.3$, red (dashed): $\xi = 0.7$.

One should keep in mind, that these values are normalised. The absolute damage inflicted for $T_{act} = 0.06s$ at the reference point X_{ref} is $D_{Xref,\xi=0.3} = 4.76 \cdot 10^{-5} s^{-1}$ for $\xi = 0.3$. For $\xi = 0.7$ it is only $D_{Xref,\xi=0.7} = 2.16 \cdot 10^{-7} s^{-1}$. As rupture of the component is expected at $D = 1$, the life expectancy at $X_g = X_{ref}$ is $T_{life} = D_{Xref}^{-1}$, if assumed that the fatigue is caused exclusively by the extreme turbulence so far examined during take-off/approach.

5 Conclusion

The influence of actuator properties onto handling qualities within the context of reduced stability for the future aircraft concept VELA has been demonstrated in this paper. In particular, the flight of the closed-loop aircraft with imposed handling qualities for the short-period oscillation in turbulent atmosphere has been analysed. As results, limits for the centre of gravity position have been derived from deflection and rate fluctuations as well as the fatigue and damage inflicted upon the actuator.

References

[1] A. P. Feuersänger, C. Toussaint, and C. Döll. The impact of reduced lateral stability on the v_{MC} equilibrium and manoeuvres during early design phases of an aircraft. *Proceedings of Deutscher Luft-und Raumfahrtkongress, DGLR, Friedrichshafen, Germany*, 2005.

[2] A.P. Feuersänger and G. Ferreres. Design of a robust back-up controller for an aircraft with reduced stability. *Proceedings of the Guidance, Navigation, and Control Conference, AIAA, Keystone/Co, USA*, 2006.

[3] F.M. Hoblit. *Gust loads on aircraft: concepts and applications*. Education Series. AIAA, 1988.

[4] C. Lalanne. *Dommages par fatigue*, volume 4 of *Vibrations et chocs mécaniques*. Hermes Science Publications, Paris, London, 1st edition, September 1999.

[5] C. Lalanne. *Vibrations aléatoires*, volume 3 of *Vibrations et chocs mécaniques*. Hermes Science Publications, Paris, London, 1st edition, September 1999.

[6] Y. Losser and P. Mouyon. Ajustement de lois de pilotage pour la réduction du dommage par fatigue des servocommandes d'un avion. In *Conférence Internationale Francophone d'Automatique CIFA 2004*, Douz, Tunisia, November 2004.

[7] Military-Specifications. Military standard - flying qualities of piloted aircraft. Technical Report MIL-STD-1797, USA.

[8] P. Mouyon and A. Gaillet. Critère de dommage par fatigue pour les servocommandes d'un avion. In *Conférence Internationale Francophone d'Automatique CIFA 2004*, Douz, Tunisia, November 2004.

[9] J.L. Pac. Les processus stochastiques. *Lecture notes, SUPAERO, Toulouse, France*.

[10] C. Toussaint, O. Renier, and L. Planckaert. Qualités de vol d'une aile volante naturellement instable. Technical Report RT 211/07505 DAAP-DCSD, ONERA Toulouse, France, 2004.